Tensile Deformation Mechanisms of Polypropylene/Elastomer Blends Reinforced with Short Glass Fiber

Sie Chin Tjong,[1] Shi-Ai Xu,[1,2] Robert Kwok Yiu Li,[1] Yiu-Wing Mai[3]

[1]*Department of Physics and Materials Science, City University of Hong Kong, Tat Chee Avenue, Kowloon, Hong Kong*
[2]*Institute of Polymer Science and Engineering, East China University of Science and Technology, 130 Mei Long Road, Shanghai 200237, China*
[3]*Center for Advanced Materials Technology (CAMT), School of Aerospace, Mechanical and Mechatronic Engineering, University of Sydney, Sydney, NSW 2006, Australia*

Received 8 January 2002; accepted 5 May 2002

ABSTRACT: Polypropylene hybrid composites reinforced with short glass fiber (SGF) and toughened with styrene–ethylene butylenes–styrene (SEBS) elastomer were prepared using extrusion and injection-molding techniques. Moreover, hybrids compatibilized with SEBS-grafted maleic anhydride (SEBS-*g*-MA) and hybrid compatibilized with PP grafted with maleic anhydride (PP-*g*-MA) were also fabricated. The matrix of the latter hybrid was designated as mPP and consisted of 95% PP and 5% PP-*g*-MA. Tensile dilatometry was carried out to characterize the fracture mechanisms of hybrid composites. Dilatometric responses showed that the elastic deformation was the dominant deformation mechanism for the SGF/SEBS/PP and SGF/SEBS-*g*-MA/PP hybrids. However, cavitation deformation prevailed over shearing deformation for both hybrids at the higher strain regime. The cavitation strain resulted from the debonding of glass fibers and from the crazing of the matrix in the SGF/SEBS/PP hybrid. In contrast, the cavitation was caused by the debonding of SEBS particles from the matrix of the SGF/SEBS-*g*-MA/PP hybrid. The use of PP-*g*-MA resulting in elastic deformation was the main mode of deformation in the low-strain region for the SGF/SEBS/mPP and SEBS/SEBS-*g*-MA/mPP hybrids; thereafter, shearing appeared to dominate at the higher strain regime. This was attributed to the MA functional group improving the bonding between the SGF and PP. The correlation between fracture morphology and dilatometric responses also is presented in the article. © 2002 Wiley Periodicals, Inc. J Appl Polym Sci 87: 441–451, 2003

Key words: polypropylene (PP); elastomers; tensile dilatometry; glass fiber; volume strain

INTRODUCTION

Polymeric materials are widely used as structural materials in many engineering fields. An important selection criterion of these materials for engineering applications is their toughness characteristics. The toughness of materials is related to their deformation behavior and fracture mechanisms. It is of practical interest to study the deformation and fracture toughening mechanisms of polymeric materials.

The deformation mechanisms of polymers in the tensile process can be explored by tensile dilatometry. This technique involves the determination of the volume change of samples during the tensile process. In general, shear deformation produces no volume change, whereas cavitation deformation, such as crazing, results in a dramatic increase in volume strain. Many researchers have used the dilatometric method to study the deformation mechanisms of polymer blends and composites.[1–22] For example, Bucknall and Clayton[19,20] used this method to analyze the creep data and to study the deformation process of rubber-toughened plastics. Similarly, Heikens and coworkers[1–7] used this concept to determine the volume strain of a specimen during tensile deformation by simultaneously measuring the axial and transverse strains. More recently, Xu and Tjong have used this technique to investigate the deformation mechanisms of polyethylene/polystyrene blends compatibilized with styrene–ethylene butylene–styrene triblock copolymer (SEBS).[21,22] Their results showed that elastic deformation is the main mode of deformation prior to yielding for PS/HDPE toughened with SEBS. Thereafter, shear and crazing appear to dominate over the elastic deformation.[22]

Polypropylene (PP) is extensively used for a variety of applications. However, PP is characterized by poor impact strength under high strain rate or low temperature environments. Its low notched toughness is not sufficient for use in engineering sectors. To improve its impact toughness, PP is usually blended with elas-

Correspondence to: S. C. Tjong (aptjong@cityu.edu.hk).
Contract grant sponsor: Research Grants Council of Hong Kong Special Administrative Region, China; contract grant number: CityU 1029/00E.

Journal of Applied Polymer Science, Vol. 87, 441–451 (2003)

tomers particles, such as SEBS, ethylene–propylene rubber (EPR), and ethylene–propylene–diene monomer (EPDM). Among these, SEBS can act as an impact modifier and a compatibilizer. Many studies have shown that the addition of SEBS improves the impact resistance of PP but significantly reduces its stiffness and yield strength.[23–26] To restore the required stiffness and strength, inorganic glass blead (GB) and filler can be incorporated into SEBS-modified PP, leading to the formation of hybrid composites.[27,28] For example, Friedrich and coworkers demonstrated that SEBS and GB particles dispersed separately in the matrix of a GB/SEBS/PP hybrid. In contrast, it was shown that SEBS tended to encapsulate GB when maleic-anhydride–grafted SEBS (SEBS-*g*-MA) was used as an elastomer compatibilizer.[28] Little information is available concerning the deformation and fracture mechanisms of glass-fiber-reinforced PP composite toughened with elastomers.

More recently, we have carried out preliminary studies on the fabrication and static tensile behavior as well as the impact behavior of a short-glass-fiber-reinforced (SGF-reinforced) PP hybrid composite toughened with SEBS or SEBS-*g*-MA. The results demonstrated that the SEBS-*g*-MA copolymer improves the yield strength and impact performance of an SGF/SEBS-*g*-MA/PP composite. This was attributed to the MA functional group, which enhances adhesion between SEBS and SGF.[29,30] The aims of the current work were to study the tensile deformation and toughening mechanisms of SGF/SEBS/PP and SGF/SEBS-*g*-MA/PP hybrids.

EXPERIMENTAL

Materials

Polypropylene (Profax 6331) used in this work was purchased from Himont Company (Thailand). Its density and melt flow index were 0.9 g/cm^{-3} and 12 g/10 min, respectively. SEBS (Kraton G1652) and SEBS-*g*-MA (Kraton FG 1901X) copolymers were kindly supplied by the Shell Company (Houston, TX). The molecular weights of the PS block and central EB block of the copolymers were 7500 and 37,500, respectively, and the PS weight fraction was 28.6%. The maleic anhydride content in Kraton FG 1901 X was 1.84 wt %. In the present study reinforcement was provided by short glass fibers about 6 mm long.

Blending

All materials used were dried separately in ovens for more than 48 h. SEBS/PP 20/80, SEBS-*g*-MA/PP 20/80 blends, and their composites reinforced with SGF were initially prepared in a Brabender twin-screw extruder. The temperature profiles were set at 180°C, 220°C, 220°C, and 210°C (from the entrance to the die). The SGF content of hybrids was fixed at 30 wt %. After compounding the extrudates were pelletized and then dried at 100°C for 48 h. Using these pellets, dog bone specimens were injection-molded using a Chen Hsong machine. The barrel zone temperature profiles were set at 200°C, 210°C, and 220°C. For purposes of comparison, pure PP and SGF/PP 30/70 composite were also prepared and injection-molded under similar conditions.

Tensile dilatometry

Tensile dilatometric measurements of smooth specimens were carried out at room temperature (21°C) using an Instron tensile tester (model 4206) under a crosshead speed of 1 mm/min. The relative humidity during the tests was 65%. In the tests two extensometers were used to measure the longitudinal and transverse strains simultaneously. The transverse dimension could be width or thickness, but only the width displacement was determined. The gauge lengths of the longitudinal and transverse extensometers were 12.5 mm and 15 mm, respectively. The sensitivity of both extensometers was 0.01%, and the accuracy of the measurements of transverse strain was 0.07%. Three measurements were made for each sample to check for the reproducibility in longitudinal and transverse strains, and the relative error was less than 0.1%. To avoid damage to the extensometers during tensile tests, the experiments were stopped on reaching the maximum yield stress. After the dilatometric test the specimens were fractured in liquid nitrogen and were coated with a thin layer of gold prior to being examined in scanning electron microscopes (SEM; JEOL JSM 820 and JEOL JSM 6335F).

RESULTS AND DISCUSSION

An increase in the volume strain of the bulk of a material resulting from the application of a tensile stress can be described as follows,[9,31,32]

$$\frac{\Delta V}{V} = (1 + \varepsilon_l)(1 + \varepsilon_w)(1 + \varepsilon_t) - 1 \qquad (1)$$

where ΔV is the change in volume; V is the original volume; the ratio $\Delta V/V$ is the volume strain; and ϵ_l, ϵ_w, and ϵ_t are, respectively, the longitudinal, transverse, and thickness engineering strains. If the material is assumed to be isotropic, the fundamental elastic constants such as modulus, E, and lateral contraction ratio, ν, are direction independent. Accordingly, the lateral contraction ratios in the width and thickness directions are equivalent[17],

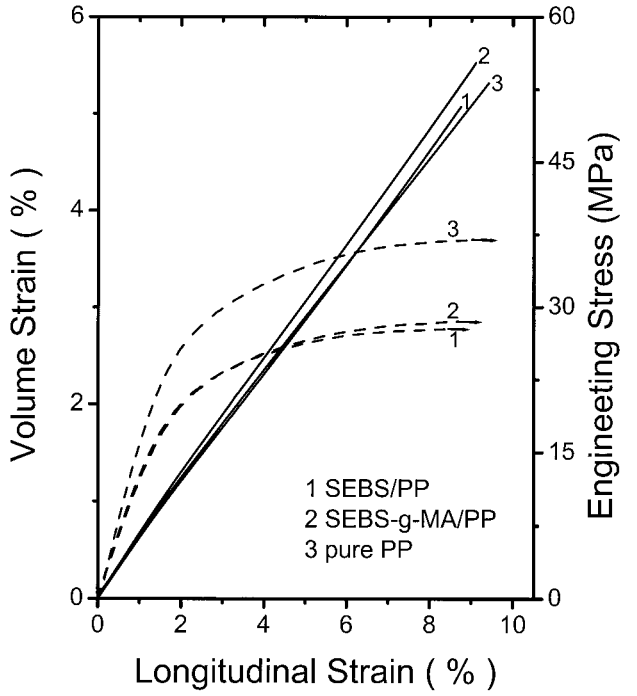

Figure 1 Engineering stress and volume strain versus longitudinal strain curves for pure PP, SEBS/PP 20/80, and SEBS-*g*-MA/PP 20/80 blends. Solid-line curves correspond to the plots of volume strain versus longitudinal strain; dashed-line curves correspond to the plots of engineering stress versus longitudinal strain.

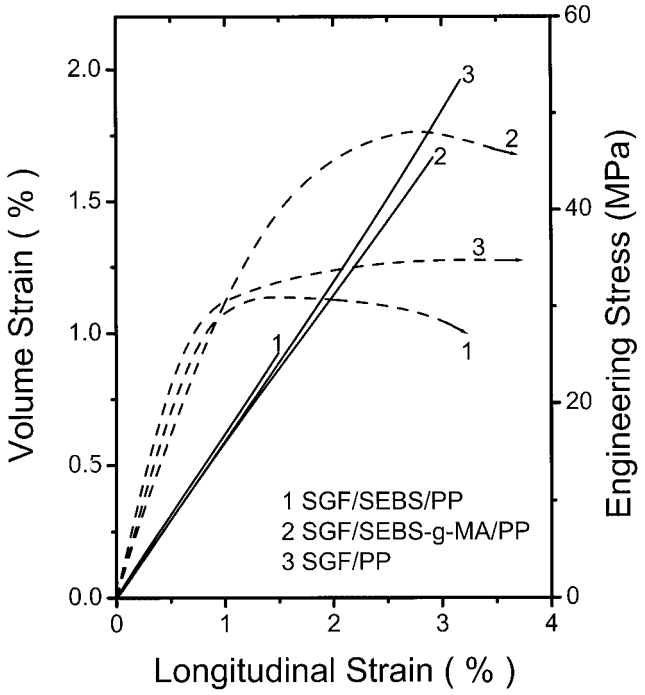

Figure 2 Engineering stress and volume strain versus longitudinal strain curves for the SGF/PP, SGF/SEBS/PP and SGF/SEBS-MA/PP composites. Solid-line curves correspond to the plots of volume strain versus longitudinal strain; dashed-line curves correspond to the plots of engineering stress versus longitudinal strain.

$$v = -\frac{\varepsilon_w}{\varepsilon_l} = -\frac{\varepsilon_t}{\varepsilon_l} \tag{2}$$

Therefore, eq. (1) can be simplified as:

$$\frac{\Delta V}{V} = (1 + \varepsilon_l)(1 + \varepsilon_t)^2 - 1 \tag{3}$$

Figure 1 shows the engineering stress and volume strain–versus–longitudinal strain curves for the pure PP, SEBS/PP 20/80, and SEBS-*g*-MA/PP 20/80 blends. All three samples exhibited yield point and necking behavior during tensile deformation. They underwent extensive plastic deformation and showed no fracture up to a strain of 910%. Figure 1 also shows that the volume strains for these samples tended to increase with increasing longitudinal elongation and that they varied almost linearly with longitudinal strain. Further, the volume strains of the PP blends containing SEBS elastomer were slightly higher than those for pure PP. This is because elastomer particles can act as stress concentrators, initiating crazes in the matrix near the periphery of particles. Figure 2 shows the engineering stress and volume strain–versus–longitudinal strain curves for the SGF/PP, SGF/SEBS/PP, and SGF/SEBS-MA/PP composites. For the SGF/

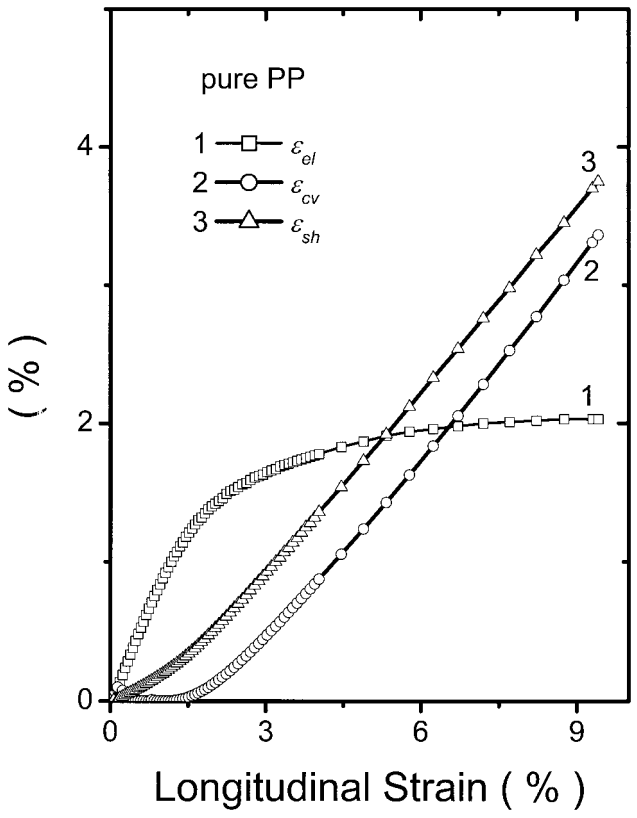

Figure 3 Plots of the elongation strains caused by elastic deformation (ϵ_{el}), cavitation (ϵ_{cv}), and shear deformation (ϵ_{sh}) versus the total elongation strain for pure PP.

SEBS/PP and SGF/PP composites, the stress reached a maximum at longitudinal strain of about 1.8% and 3%, respectively. For the SGF/SEBS-MA/PP hybrid, a yield stress was observed when the longitudinal strain reached about 4%. And the incorporation of maleated SEBS into the SGF/PP composite enhanced the yield stress dramatically. It can also be seen from Figure 2 that the volume change–versus–longitudinal strain was linear for the SGF/PP, SGF/SEBS/PP, and SGF/SEBS-MA/PP composites.

In the small deformation limit the normal hydrostatic and deviatioric components of applied stress can be analyzed.[17] The hydrostatic stress yields an increase in the volume in the dilational response of the material, whereas the deviatioric (shear) stress results in a change of shape not volume. To determine the contributions of various deformations (i.e., elastic, shear, and cavitation) to the total longitudinal elongation, a quantitative model proposed by Heikens et al. was adopted in this study.[31,32] In this model the respective contributions of elastic deformation, shear deformation, and cavitation to the total elongation strain and the total volume strain are assumed to be additive. Cavitation includes all deformation processes that lead to an increase in volume strain, such as crazing, cavitation of rubber particles, and debonding of reinforcing filler at the interfaces. It is assumed that shear deformation makes a negligible contribution to the volume strain and that the volume strain caused by cavitation is equal to the elongation strain. It must be pointed out that the important criterion that determines the use of this model is that the specimen must elongate uniformly throughout the entire gauge portion.[4] This means that this model may only be applied to polymer specimens prior to necking.

According to this model, at any elongation strain the strains caused by elastic deformation (ε_{el}), shear deformation (ε_{sh}), and cavitation deformation (ε_{ca}) can be calculated from σ_T-ε-$\Delta V/V$ diagrams and are given by the following equations:

$$\varepsilon_{el} = \frac{\sigma_T}{E} \tag{4}$$

$$\varepsilon_{cv} = \frac{\Delta V}{V} - \frac{(1-2v)\sigma_T}{E} \tag{5}$$

$$\varepsilon_{sh} = \varepsilon - \frac{\Delta V}{V} - \frac{2v\sigma_T}{E} \tag{6}$$

where σ_T is the true stress, E is Young's modulus, ε is the elongation strain, and ν is the Poisson ratio. E and ν can be determined from the initial slopes of the

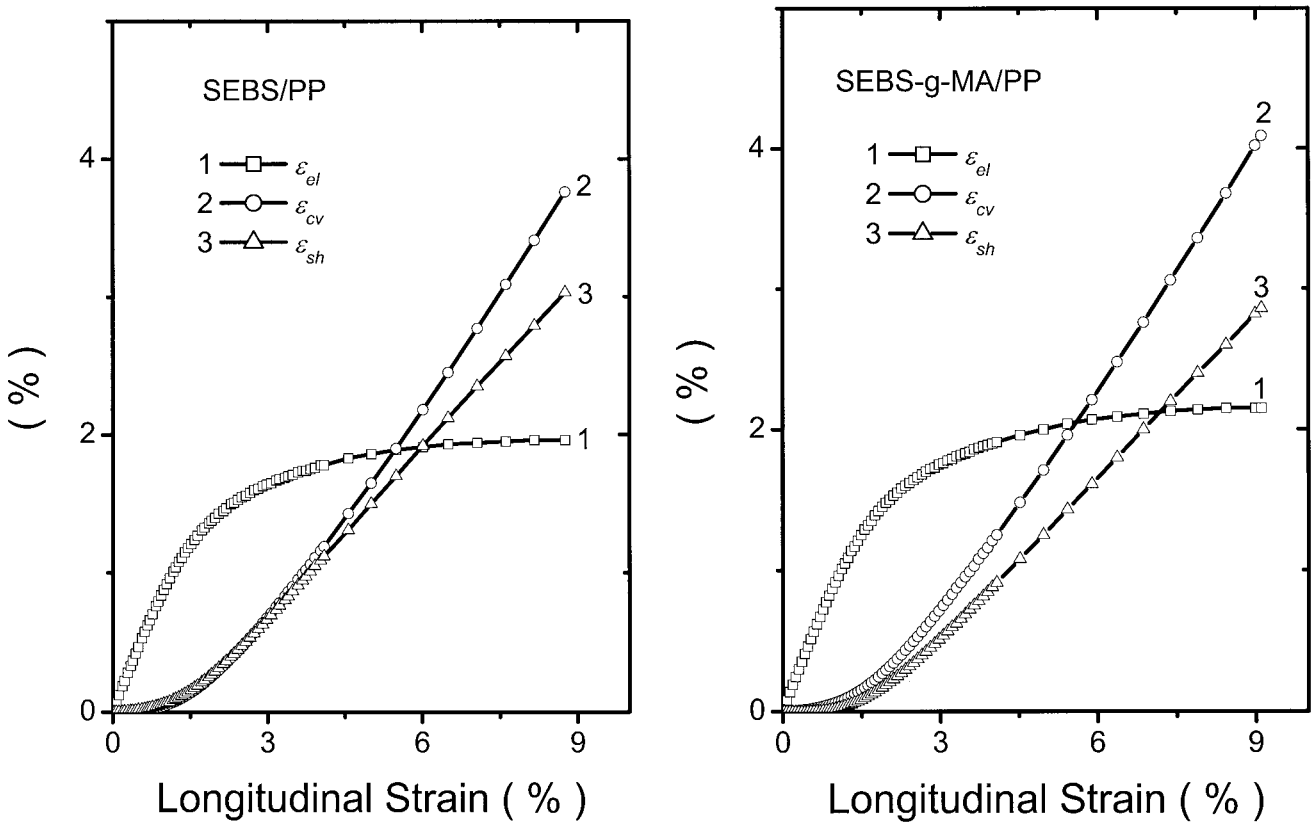

Figure 4 Plots of the elongation strains caused by elastic deformation (ε_{el}), cavitation (ε_{cv}), and shear deformation (ε_{sh}) versus the total elongation strain for (a) SEBS/PP and (b) SEBS-*g*-MA/PP blends.

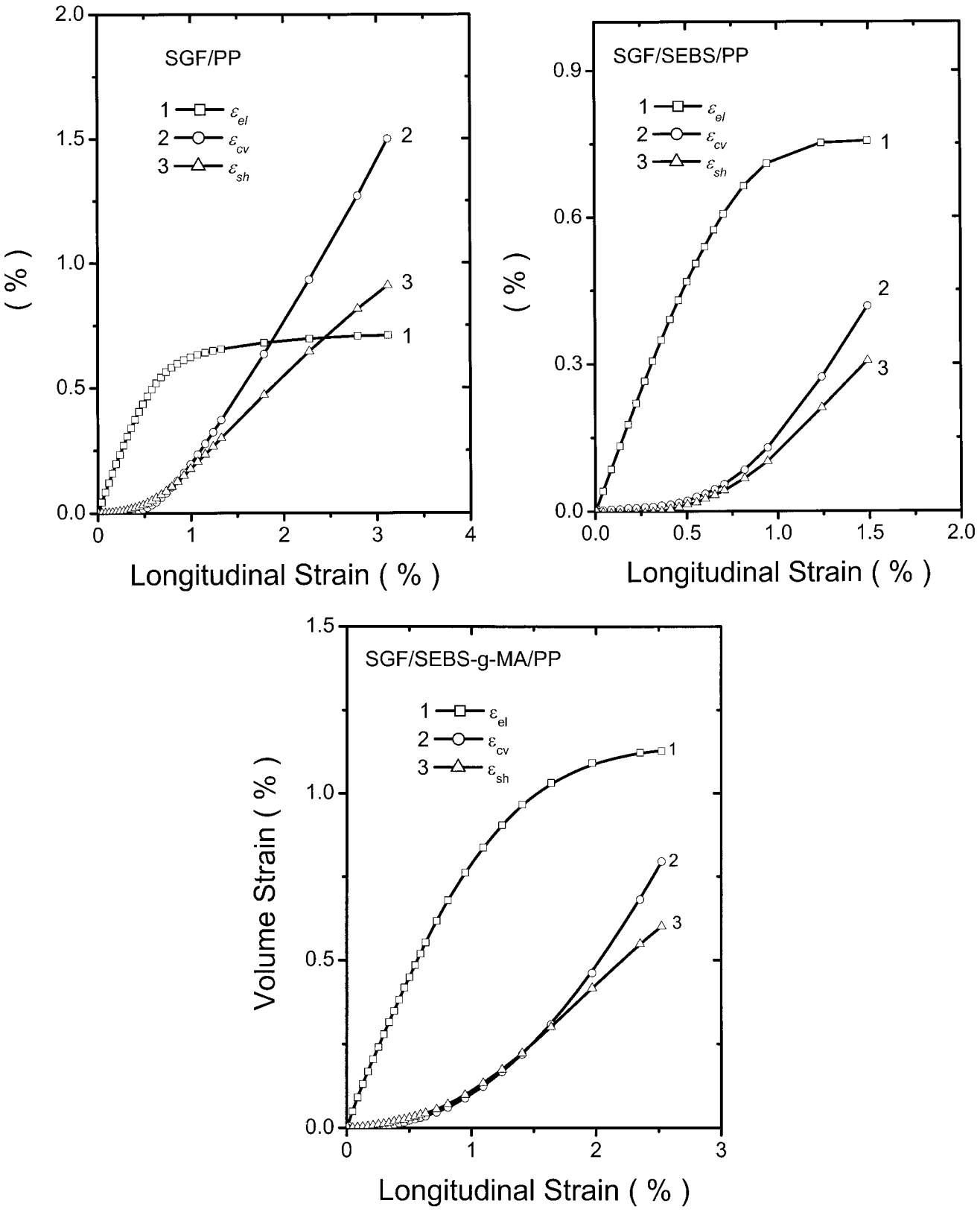

Figure 5 Plots of the elongation strains caused by elastic deformation (ε_{el}), cavitation (ε_{cv}), and shear deformation (ε_{sh}) versus the total elongation strain for (a) SGF/PP, (b) SGF/SEBS/PP, and (c) SGF/SEBS-*g*-MA/PP composites.

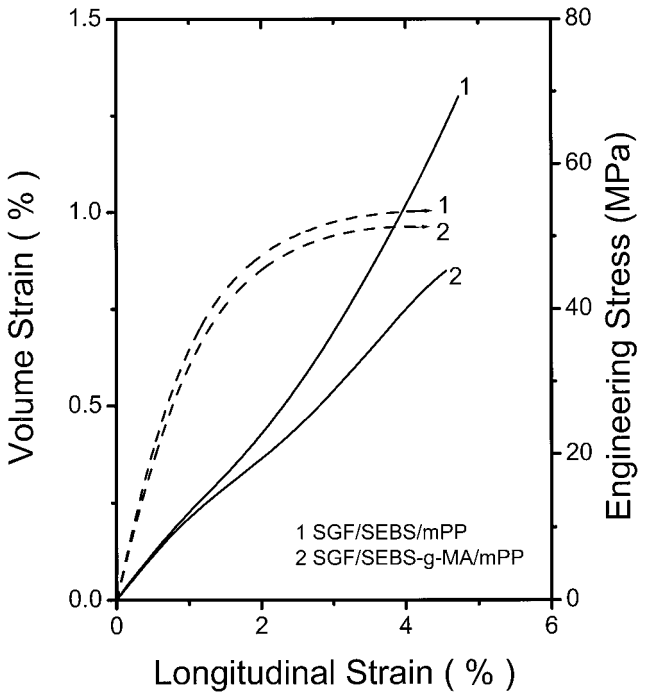

Figure 6 Engineering stress and volume strain versus longitudinal strain curves for the SGF/SEBS/mPP and SGF/SEBS–MA/mPP composites. Solid-line curves correspond to the plots of volume strain versus longitudinal strain; dashed-line curves correspond to the plots of engineering stress versus longitudinal strain.

σ_{eng}–ε (ε_{eng} is the engineering stress) and ε_t–ε curves, respectively. The true stress is calculated using the instantaneous cross-sectional area over which the deformation occurs. The relation between the true and engineering stress is

$$\sigma_T = \frac{\sigma_{eng}}{(1 - \varepsilon_t)^2} \tag{7}$$

The elongation strains caused by the elastic deformation, shear deformation, and cavitation process as a function of the total longitudinal strain for pure PP are shown in Figure 3. It can be seen that the elastic deformation predominates in the low-strain range and that shear and cavitation become the dominant deformation modes in high-strain range. For pure PP the cavitation deformation is associated with crazing only. Moreover, shear deformation predominates over crazing, and this is a general deformation characteristic for semicrystalline polymer. Figure 4(a,b) shows the separate contributions of the three deformations during the tensile process for the SEBS/PP and SEBS-*g*-MA/PP blends. Apparently, elastic deformation was the main deformation mode in the lower strain range. In contrast with pure PP, cavitation deformation predominated over shearing for these two blends, and the

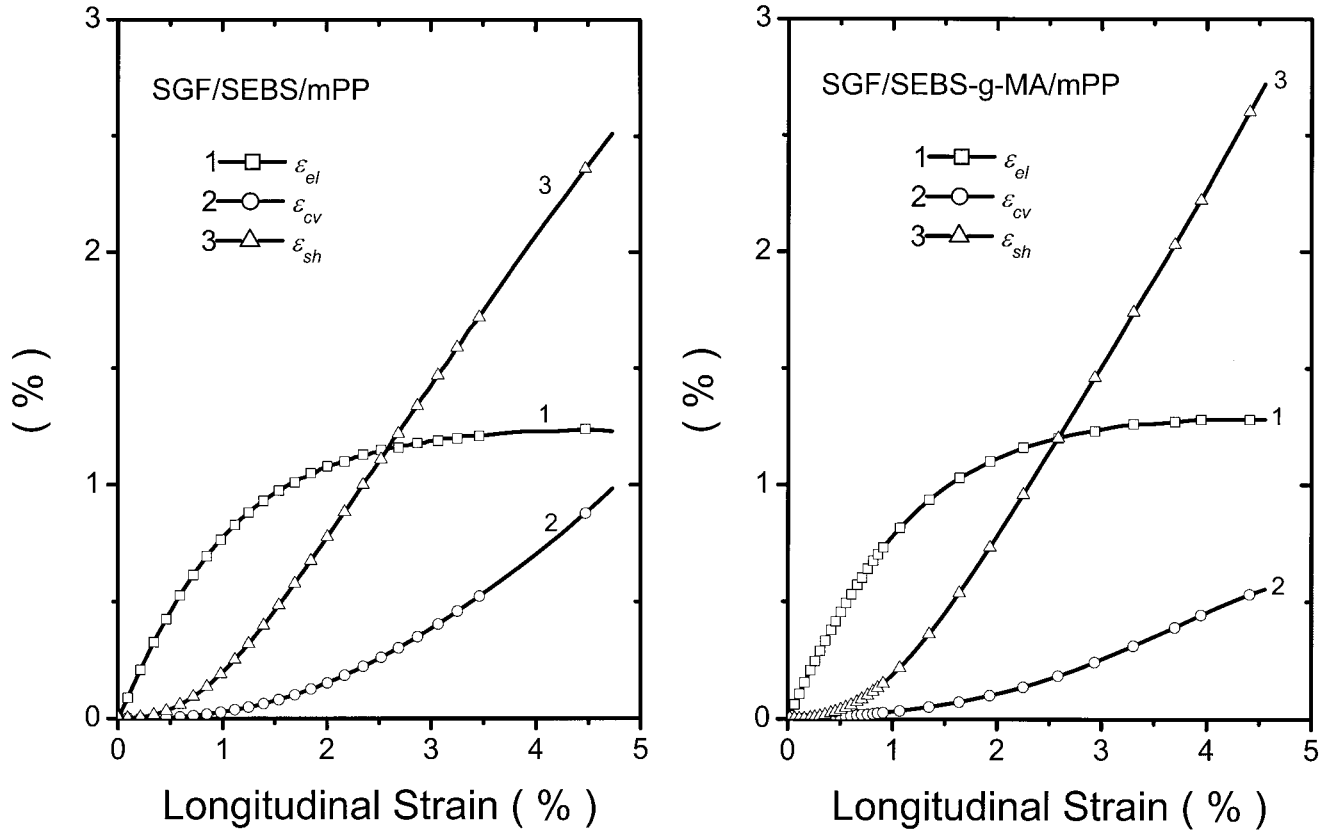

Figure 7 Plots of the elongation strains caused by elastic deformation (ε_{el}), cavitation (ε_{cv}), and shear deformation (ε_{sh}) versus the total elongation strain for (a) SGF/SEBS/mPP and (b) SGF/SEBS-MA/mPP hybrids.

TABLE I
Specific Essential Work of Fracture and Specific Plastic Work for Hybrids

Sample	w_e (kJ/m^2)	βw_p (kJ/m^2)
SGF/SEBS/PP	29.20	2.42
SGF/SEBS-*g*-MA/PP	11.55	1.28
SGF/SEBS/mPP	7.81	2.92
SGF/SEBS-*g*-MA/mPP	7.85	2.11

trend became more obvious for SEBS-*g*-MA/PP blends.

Figure 5(a–c) shows the plots of elongation strains from elastic deformation, shear deformation, and cavitation deformation versus the total elongation strain for the SGF/PP, SGF/SEBS/PP and SGF/SEBS-*g*-MA/PP composites, respectively. Figure 5(a) reveals that the elastic deformation is the dominant deformation mechanism at low strains. Thereafter, cavitation deformation associated with the debonding of SGF from PP matrix predominates over shearing at a higher strain range. Such a deformation mode is expected because the SGF and PP has poor adhesion bonding. In contrast, the elastic deformation is the dominant deformation mechanism for the SGF/SEBS/PP and SGF/SEBS-*g*-MA/PP hybrids over the total strain range studied [Fig. 5(b,c)]. The shearing and cavitation deformation strains are much smaller compared with the elastic strain. The cavitation deformation obviously predominates over the shear deformation in the higher strain region. The cavitation strain in the SGF/SEBS/PP hybrid arises from the interfacial bonding between the SGF and SEBS, and between SGF and PP it is relatively weak. When this hybrid is stressed, debonding between the SGF and SEBS and between the SGF and PP occurs readily, leading to the formation of voids or cavitation.

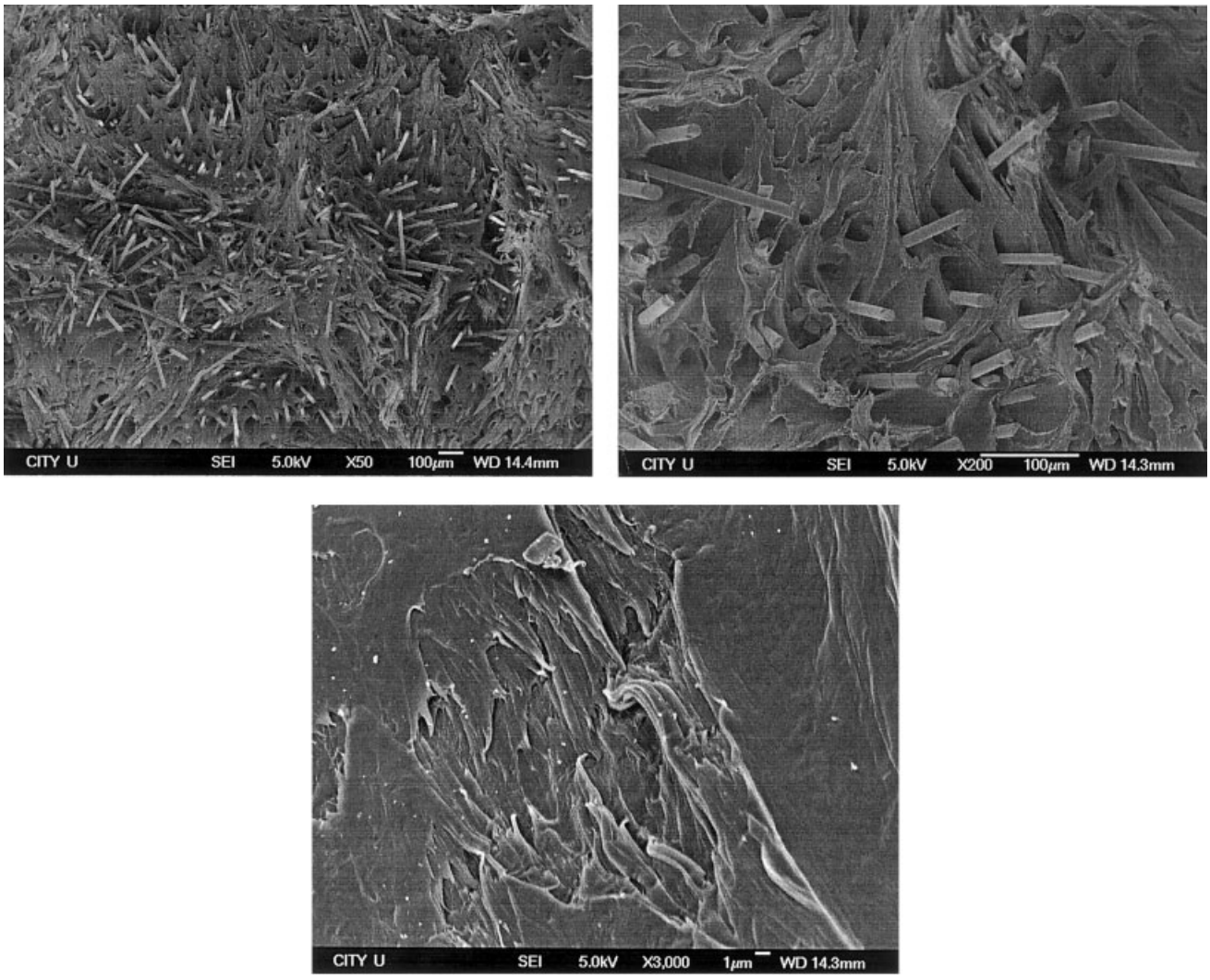

Figure 8 SEM micrographs showing the fracture morphologies the SGF/SEBS/PP hybrid subjected to dilatometric test: (a) low-magnification fractograph; (b) higher magnification view showing formation of voids at the glass-fiber interface associated with debonding and pullout of fibers; (c) higher magnification view showing crazes in the matrix of hybrid.

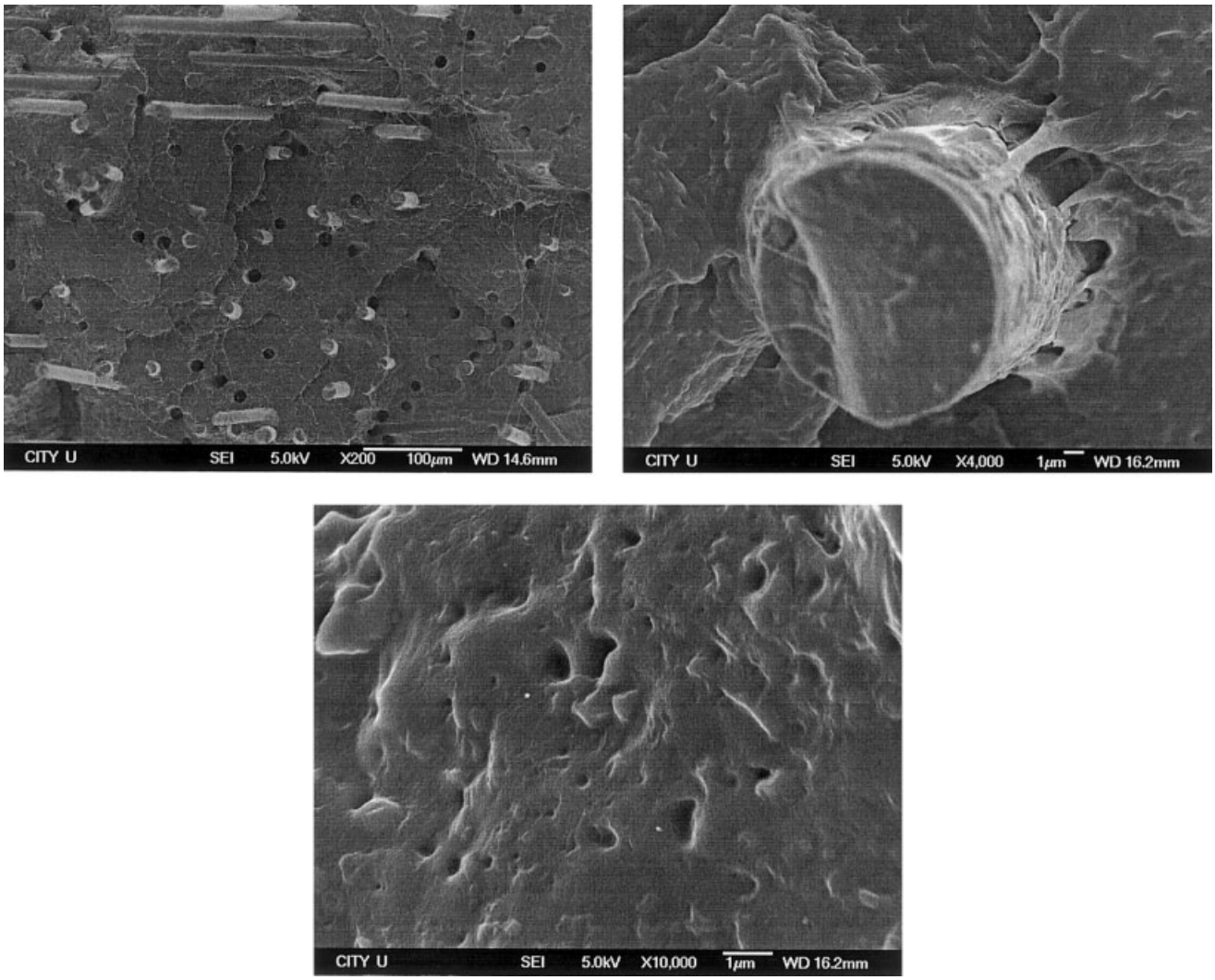

Figure 9 SEM micrographs showing the fracture morphologies the SGF/SEBS-*g*-MA/PP hybrid subjected to dilatometric test: (a) low magnification fractograph; (b) higher magnification view showing formation of cavities at the glass-fiber interface; and (c) higher magnification view showing fine cavities in the matrix of hybrid associated with debonding of elastomers from the matrix.

The interfacial bonding developed in the SGF/SEBS/PP and SGF/SEBS-*g*-MA/PP hybrids is rather complex. It could arise from the interaction between SGF and SEBS (or SEBS-*g*-MA), between SGF and PP, or between PP and SEBS (or SEBS-*g*-MA). The interfacial bonding between SGF and SEBS can be enhanced by employing maleated SEBS.[29] This is because the MA functional group grafted to the EB midblock of SEBS can react with hydroxyl groups on the glass fiber surfaces during compounding, thereby improving compatibility between the SGF and SEBS.[29] The interaction between SGF and PP is limited because SGF has a polar surface and PP is a nonpolar polyolefin. For the PP and SEBS interface, physical interactions can take place between SEBS and PP, though PP and PS are incompatible. The interaction arises because the chemical structure of PP is close to the midblock of SEBS. Accordingly, the EB midblock of SEBS can diffuse into the PP phase, forming small micelles.[25] From these it appears that a stronger bonding can be developed between the SGF and SEBS elastomer for the SGF/SEBS-*g*-MA/PP hybrid. Void formation because of the debonding of the glass fiber is more restricted. It is considered that the cavitation process as shown in Figure 5(c) is derived from the debonding of glass fiber from the PP interface.

As mentioned above, the interaction between the SGF and PP is limited. To enhance their interaction, PP-*g*-MA is used as a compatibilizer for the composites. Accordingly, mPP was prepared by blending 95% PP with 5% PP-*g*-MA. The effect of the PP-*g*-MA compatibilizer on the dilational responses of the SGF/SEBS/mPP and SGF/SEBS-*g*-MA/mPP hybrid composites is shown in Figure 6. The respective contributions of various deformations for the SGF/SEBS/mPP and SGF/SEBS-*g*-MA/mPP hybrid composites are

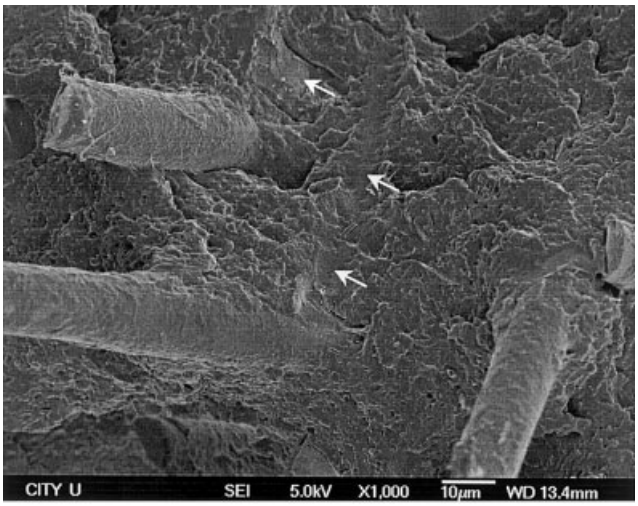

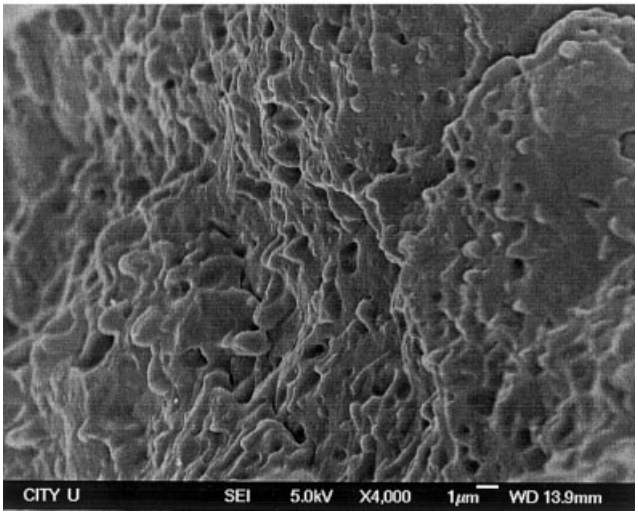

Figure 10 SEM micrographs of the SGF/SEBS/mPP hybrid subjected to dilatometric test showing (a) flat and deform regions in the matrix and (b) higher magnification view of the matrix region undergoes shear deformation. Arrows in (a) indicate flat morphology.

shown, respectively, in Figure 7(a,b), which reveals that the mechanism that prevails in the SGF/SEBS/mPP and SGF/SEBS-*g*-MA/mPP hybrids immediately after elastic deformation is shear yielding. This is because stronger interactions are developed between the SGF and PP from the incorporation of the PP-*g*-MA compatibilizer. Consequently, the debonding of the SGF from the matrix is restricted. In other words, the degree of bonding between the SGF with SEBS and PP phases controls the deformation mechanism during the tensile process.

Fracture toughness

In previous studies[30,33] we used the essential work of fracture (EWF) concept to evaluate the fracture toughness of the SGF/SEBS/PP, SGF/SEBS-*g*-MA/PP, SGF/SEBS/mPP, and SGF/SEBS-*g*-MA/mPP hybrids. The approach involves the use of samples having sharp cracks, that is, double-edge notch tension specimens (DENT) subjected to tensile deformation. According to this method, the total work of fracture (W_f) of ductile polymer having a sharp crack can be divided into the essential work of fracture (W_e) and the nonessential plastic work (W_p). The former is the energy required to fracture the polymer in its process zone, which creates two new fracture surfaces, whereas the latter is the energy dissipated in the plastic zone during crack propagation. W_e essentially is a surface energy and W_p a volume energy. Mathematically, W_f can be written in terms of the related specific work terms:

$$w_f = \frac{W_f}{Lt} = w_e + \beta w_p L \tag{8}$$

where w_f is the specific total fracture work, w_e and w_p are the specific essential fracture work, and the specific plastic work, respectively; L is ligament length, t is thickness of specimen, and β is a shape factor of the plastic zone. Accordingly, w_e and βw_p can be determined from the ordinate intercept and slope of the linear regression plot of w_f versus L. Table I summarizes the w_e and βw_p values of hybrids determined from the EWF approach.[30,33] Table I reveals that the SGF/SEBS/PP composite without MA functional group exhibits a much higher fracture toughness than other maleated hybrids. This implies that stronger bonding between SGF and PP or between SGF and SEBS is detrimental to the fracture toughness of hybrids toughened with elastomers. Tjong et al. reported that the high fracture toughness of SGF/SEBS/PP hybrid derives from the debonding and pullout of glass fibers from the PP matrix. However, the pullout of glass fibers from the PP matrix is restricted in the SGF/SEBS-*g*-MA/PP, SGF/SEBS/mPP, and SGF/SEBS-*g*-MA/mPP hybrid composites, leading to a lower fracture toughness.[30,33]

Fractography

Figure 8(a–c) shows the SEM fractographs of the SGF/SEBS/PP hybrid subjected to a dilatometric test. Numerous voids associated with the debonding and pullout of fibers can be readily seen in the fractographs [Fig.8(a,b)]. Moreover, crazes are also evident in some areas of the matrix [Fig. 8(c)]. The debonding voids and crazes contribute to the cavitation strain, as depicted in Figure 5(b). And the cavitation predominates over shear yielding. Accordingly, glass fiber debonding and pullout are the main energy dissipation mechanisms for the SGF/SEBS/PP hybrid. For the SGF/SEBS-*g*-MA/PP hybrid, some glass fibers are firmly

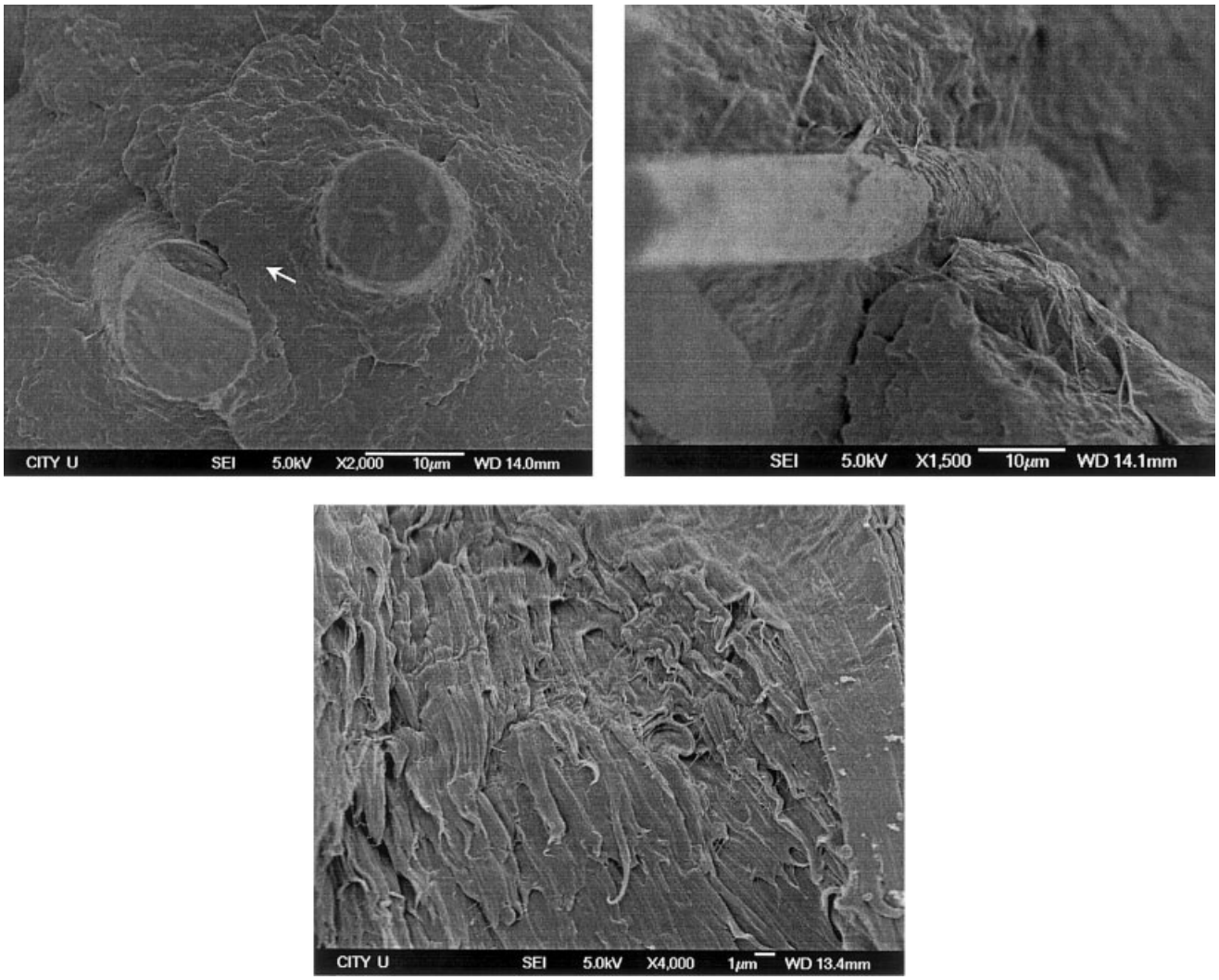

Figure 11 SEM micrographs of the SGF/SEBS-*g*-MA/mPP hybrid subjected to dilatometric test showing (a) flat and deform regions in the matrix, (b) shear deformation at the fiber-matrix interface, and (c) higher magnification view of the matrix region undergoes shear deformation.

adhered to the matrix because the MA functional group improves adhesion between SGF and SEBS [Fig. 9(a)]. The pullout of the glass fiber in this hybrid also takes place via the cavitation process [Fig. 9(b)], but it is more restricted compared with that of the SGF/SEBS/PP hybrid. In this case, the cavitation strain as shown in Figure 5(c) derives from the debonding of the SEBS elastomer from the PP matrix. As mentioned above, physical interactions can take place between SEBS and PP because the EB midblock of SEBS can diffuse into the PP phase, forming small micelles. However, grafting of the MA functional group to SEBS increases the polarity of the EB midblock, thereby restricting the mobility of the block copolymer.[29] The incorporation of SEBS-*g*-MA improves the bonding between the SGF and SEBS at the expense of the adhesion between SEBS and PP. Accordingly, SEBS elastomers with an average size of about 0.18 μm[29] can detach more easily from the matrix of the SGF/SEBS-*g*-MA/PP hybrid, leading to the formation of fine voids, as shown in Figure 9(c).

Figures 10(a,b) and 11(a–c) show the SEM fractographs of, respectively, the SGF/SEBS/mPP and SGF/SEBS-*g*-MA/mPP hybrids subjected to the dilatometric test. It is apparent that the number of voids associated with the pullout of particles is significantly reduced in these specimens because a strong bonding developed between the PP and SEBS, particularly for the SGF/SEBS-*g*-MA/mPP hybrid. Once the SEBS particles debond from the matrix, they trigger shear deformation [Figs. 10(b) and 11(c)]. However, some regions in the matrix that do not undergo shearing appear flat [Figs. 10(a) and 11(a)]. It should be noted that a strong interfacial bonding also developed between the SGF and PP in these hybrids, leading to some matrix materials adhering to the SGF surfaces [Figs. 10(a) and 11(b)]. A careful examination of the fractographs reveals that the glass fibers fracture dur-

ing dilatometric tests because of strong interfacial bonding between SGF and PP [Fig. 11(a)]. It can be concluded that the SEM fractographic analyses correlate well with the dilatometric measurements.

CONCLUSIONS

Tensile dilatometry is a potential technique to characterize the deformation mechanisms of composites. The measurements indicate that the cavitation mechanism prevails in the SGF/PP composite after the initial elastic deformation. Voids originate from the debonding of glass fiber from PP matrix contribute to the cavitation strain in the SGF/PP composite. In contrast, the elastic deformation is the dominant deformation mechanism for the SGF/SEBS/PP and SGF/SEBS-*g*-MA/PP hybrids. However, cavitation predominates over shearing deformation for the SGF/SEBS/PP and SGF/SEBS-*g*-MA/PP hybrids at a higher strain regime. The use of PP-*g*-MA enhances the adhesion between the SGF and PP, leading to shear deformation becoming the dominant deformation mechanism at higher elongation strain. SEM fractographic analyses were in good agreement with the tensile dilatometric results.

References

1. Coumans, W. J.; Heikens, D. Polymer 1981, 21, 957.
2. Coumans, W. J.; Heikens, D.; Sjoerdsma, S. D. Polymer 1981, 21, 103.
3. Dekkers, M. E. J.; Heikens, D. J Appl Polym Sci 1983, 28, 3809.
4. Dekkers, M. E. J.; Heikens, D. J Appl Polym Sci 1985, 30, 2389.
5. Dekkers, M. E. J.; Heikens, D. J Mater Sci 1985, 20, 3873.
6. Dekkers, M. E. J.; Hobbs, S. Y.; Watkins, V. H. J. Mater Sci 1988, 23, 1225.
7. Hobbs, S. Y.; Dekkers, M. E. J. J Mater Sci 1989, 24, 1316.
8. Bucknall, C. B.; Clayton, D.; Keast, W. J Mater Sci 1972, 7, 1443.
9. Bucknall, C. B.; Clayton, D.; Keast, W. J Mater Sci 1973, 8, 514.
10. Bucknall, C. B.; Drinkwater, I. C. J Mater Sci 1972, 8, 1800.
11. Bucknall, C. B.; Stevens, W.W. J Mater Sci 1980, 15, 2950.
12. Bucknall, C. B.; Page, C. J. J Mater Sci 1982, 17, 808.
13. Bucknall, C. B.; Clayton, D.; Keast, W. J Mater Sci, 1984, 19, 2064.
14. Bucknall, C. B.; Davies, P.; Partridge, J. K. J Mater Sci 1986, 21, 307.
15. Bucknall, C. B.; Heather, P. S.; Lazzeri, A. J Mater Sci 1989, 24, 2255.
16. Hutchinson, J. M.; Bucknall, C. B. Polym Eng Sci 1980, 20, 173.
17. Naqui, S. I.; Robinson, I. M. J Mater Sci 1993, 28, 1421.
18. Schwarz, J. M. C.; Keskkula, H.; Barlow, J. W.; Paul, D. R. J Appl Polym Sci 1988, 35, 653.
19. Bucknall, C. B.; Clayton, D. J Mater Sci 1972, 7, 202.
20. Bucknall, C. B.; Clayton, D. Nature 1971, 231, 107.
21. Xu, S. A.; Chan, C. M. Polymer J 1998, 30, 552.
22. Xu, S. A.; Tjong, S. C. J Appl Polym Sci 1999, 77, 2024.
23. Gupta, A. K.; Purwar, S. N. J Appl Polym Sci 1986, 31, 535.
24. Bassani, A.; Pessan, L. A.; Hage E. J Appl Polym Sci 2001, 82, 2153.
25. Setz, S.; Stricker, F.; Kressler, J.; Duscher, T.; Mulhaupt R. J Appl Polym Sci 1996, 59, 1117.
26. Veenstra, H.; van Lent, B. J.; van Dam, J.; de Boer, A. P. Polymer 1999, 40, 6661.
27. Stricker, F.; Mulhaupt, R. J Appl Polym Sci 1996, 62, 1799.
28. Stricker, F.; Friedrich, C.; Mulhaupt, R. J Appl Polym Sci 1998, 69, 2499.
29. Tjong, S. C.; Xu, S. A.; Li, R. K. Y.; Mai, Y. W. J Appl Polym Sci 2002, 86, 1303.
30. Tjong, S. C.; Xu, S. A.; Li, R. K. Y.; Mai, Y. W. Polym Int, to appear.
31. Heikens, D.; Sjoerdsma, S. D.; Coumans, W.J. J Mater Sci 1973, 8, 514.
32. Heikens, D.; Sjoerdsma, S. D.; Coumans, W. J. J Mater Sci 1981,16, 429
33. Tjong, S. C.; Xu, S. A.; Li, R. K. Y.; Mai, Y. W. Compos Sci Technol 2002, 62, 831.